Microstructure of Magnetron Sputtered Amorphous SiO x Films: Formation of Amorphous Si Core– Shell Nanoclusters

ARTICLE *in* THE JOURNAL OF PHYSICAL CHEMISTRY C · FEBRUARY 2010

Impact Factor: 4.77 · DOI: 10.1021/jp906284f

4 AUTHORS, INCLUDING:

Sam Zhang
Nanyang Technological University
177 PUBLICATIONS **3,810** CITATIONS

SEE PROFILE

Ming Yang
Nanyang Technological University
23 PUBLICATIONS **170** CITATIONS

SEE PROFILE

Microstructure of Magnetron Sputtered Amorphous SiO_x Films: Formation of Amorphous Si Core−Shell Nanoclusters

Wa Li Zhang

School of Mechanical and Aerospace Engineering, Nanyang Technological University, 50 Nanyang Avenue, Singapore 639798

Sam Zhang*

School of Mechanical and Aerospace Engineering, Nanyang Technological University, 50 Nanyang Avenue, Singapore 639798

Ming Yang

School of Electrical and Electronic Engineering, Nanyang Technological University, 50 Nanyang Avenue, Singapore 639798

Tu Pei Chen

School of Electrical and Electronic Engineering, Nanyang Technological University, 50 Nanyang Avenue, Singapore 639798

Received: July 3, 2009; Revised Manuscript Received: November 17, 2009

The microstructures of the as-sputtered amorphous silicon-rich oxide (SiO_x) films were investigated by using a combination of X-ray photoelectron spectroscopy (XPS) and Raman microscopy. XPS analysis reveals that the as-sputtered amorphous SiO_x films are chemically inhomogeneous. Raman spectra and valence band XPS spectra suggest the formation of amorphous Si nanoclusters in the as-sputtered amorphous SiO_x films. The size of these nanoclusters depends on the Si concentration in the films. The formation of amorphous Si nanoclusters was attributed to the high kinetic energy and surface migration of the sputtered Si atoms. It is found that the as-sputtered amorphous SiO_x films have a complex structure consisting nanoscale cluster of amorphous Si core with suboxides shell embedded in the amorphous SiO_2 matrix.

1. Introduction

Although it is difficult for bulk silicon to emit visible photoluminescence (PL) at room temperature (RT) due to its indirect bandgap nature,[1] visible PL at RT has been observed in Si nanostructures.[2−5] This property of Si nanostructures has drawn much attention because of the potential applications in development of integrated optoelectronics devices based on current Si technologies.[6−8] Si nanocrystal (nc-Si) embedded SiO_2 film (or nc-Si/a-SiO_2) is one of the most popular Si nanostructures for such optoelectronic applications. The standard approaches of synthesizing nc-Si include ion implantation of silicon into an amorphous SiO_2 matrix[9] or deposition of Si substoichiometric oxide SiO_x films using chemical vapor deposition (CVD),[8,10,11] sputtering,[12−14] or reactive evaporation.[6,15] A high-temperature annealing step is usually adopted for the segregation of the excess Si. The induced Si nanoparticles can be amorphous or nanocrystalline depending on the annealing temperature. The origin of the visible PL signals at RT is still an open question and was commonly attributed to the quantum confinement of nc-Si,[6,12,16] defects,[6,11,14,17] or Si suboxides.[18] The nc-Si size-dependent PL spectra, ranging at 680−1000 nm, are attributed to the quantum-confinement effects of excitions caused by their spatial confinement within the nc-Si after annealing at higher than 1000 °C.[6,12,16] For annealing temperature lower than 1000 °C, nanocrystalline Si may not form.[10] However, the PL signals have also been observed, believing to come either from the defects within the SiO_2[6,17] or the interface between the nanocrystals and SiO_2 matrix.[14,18] Besides, it has been reported that amorphous Si nanoclusters might be formed in the as-deposited SiO_x films.[19,20] The light emission from these as-deposited SiO_x films was attributed to the amorphous Si nanoclusters[19,20] rather than previously believed defects. Hence, a clear understanding concerning the nanoscale structure of the as-deposited SiO_x films is desirable in order to clarify the luminescence mechanism. Widely accepted knowledge concerning the microstructure of the as-deposited amorphous SiO_x is still not yet available due to the complexity of various dynamic process associating with different deposition techniques and resulting complex bonding configuration of the as-deposited films. Knowledge of the microstructure of amorphous SiO_x films has been mainly obtained from that of bulk SiO_x. There exist at least two main models of the atomic structure of amorphous SiO_x, based on both experimental and theoretical studies, the "random bonding model" (RBM)[21] and the "random mixture model" (RMM).[22] In RBM, the local bonding was considered statistical in nature and was characterized by five different local bonding possibilities: $Si-Si_{4-w}O_w$, where $w = 0, 1, 2, 3, 4$, whereas RMM assumes nanoscale regions of SiO_x is dominated by Si−Si or by Si−O bonding.[22] In addition, for bulk amorphous SiO_x, an interface clusters mixture model has also been proposed. This model assumes that the SiO_x powder contains

* To whom correspondence should be addressed. Phone: +65 67904400. Fax: +65 6791 1859. E-mail: msyzhang@ntu.edu.sg.

10.1021/jp906284f
Published on Web 01/22/2010

clusters of silicon dioxide and clusters of silicon. These Si and SiO_2 clusters are separated by interface layers of Si suboxides.[15,23]

Magnetron sputtering technique is a promising approach for the deposition of SiO_x films because of the resulted dense films and the full compatibility with mainstream Si-based technology.[14] The high kinetic energy of the sputtered atoms will result in highly compact SiO_x films with unique microstructure. So far, there is still a lack of systemic investigations on the microstructure of the as-deposited amorphous SiO_x films by magnetron sputtering, especially for its local bonding structure in the nanoscale, i.e., the bonding configuration and distribution of the silicon, oxygen, and phase separation. A model concerning the local bonding structure will be great help in the interpretation of the nc-Si growth mechanism and light emission mechanism. This paper reports a systematic investigation on the nanoscale microstructure of magnetron sputtered amorphous SiO_x films and proposes a possible model for its local bonding configuration. Quantification analysis of the X-ray photoelectron spectroscopy (XPS) spectrum reveals that the structure of the as-deposited films follows neither the bonding configuration predicted by RMB nor that predicted by RMM but exhibits the features of both models. Moreover, the results from valence band XPS spectrum and Raman spectra demonstrate the formation of nanoscale Si clusters in the as-deposited samples. The formation of Si nanoclusters in the as-deposited SiO_x films is ascribed to the high kinetic energy of the sputtered Si atoms. The local nanoscale structure of the as-sputtered $SiOx$ films consists nanocluster of amorphous Si core with suboxide shell which themselves embedded in the SiO_2 matrix.

2. Experimental Details

A reactive radio frequency (13.6 MHz) magnetron sputtering system was employed to deposit the SiO_x films from a Si target (four inch, 99.999% in purity) in a gas mixture of Ar/O_2 at a controlled gas flow rate. The substrates used in this study were p-type Si (100) wafers. Prior to deposition, the wafers were ultrasonically cleaned consecutively in acetone and ethanol for 20 min each followed by rinsing in deionized water. The Si target was placed 80 mm above the substrate, and the base pressure of the chamber was lower than 1.0×10^{-5} Pa. During deposition, the target power and sputtering pressure were fixed at 200 W and 0.2 Pa, respectively. The variation of the Ar/O_2 flow rate ratio was achieved by varying the oxygen flow rate between 0.8 and 3.0 sccm while the Ar flow was fixed at 40 sccm. No additional heat was applied on the substrate during deposition; the substrate temperature was effective 45 ± 3 °C due to ions bombardment. To remove the possible contaminations, the target was presputtered for 15 min, and the substrates were pre-etched for 15 min before the target shutter is open to allow commencement of deposition. Samples were produced by growing 200−300 nm of SiO_x layer with the composition varying from $SiO_{0.6}$ to SiO_2. The post deposition annealing was carried out at 400, 700, and 1000 °C in a rapid thermal annealing (RTA) system for 300 s. To avoid possible oxidation during annealing, first the RTA chamber was pumped down to 2.0×10^{-1} Pa, and then Ar was introduced as the protection ambient at a flow rate of 2000 sccm. The composition and chemical states of the films were determined by XPS analysis using a Kratos-Axis spectrometer with monochromatic Al Kα (1486.71 eV) on plain-view samples at a normal take off angle. To avoid the influence of surface oxidation and contaminations during sample transfer, XPS tests were conducted after removal of surface layer using Ar ion etching for 2 min (~5 nm) at 15 keV. A charge neutralizer was used to neutralize charge accumulation during test. The survey scans and high-resolution spectra were acquired using pass energies of 160 and 40 eV, respectively. The XPS spectra have been calibrated using the energy position of O 1s core-level (532 eV). Deconvolution of the XPS curves was conducted by using a fitting procedure based on the summation of Gaussian functions after Shirley background subtraction. The crystallinity of the film was characterized using Raman spectroscopy (Renishaw 1000 Ramascope system) with 633-nm line excited by He−Ne laser.

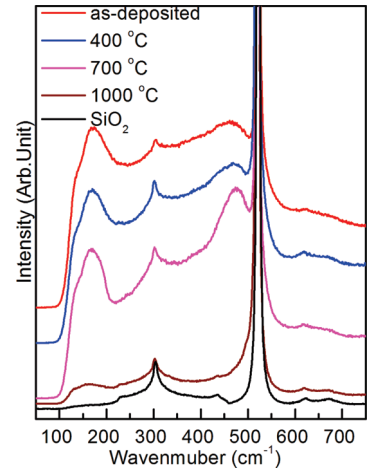

Figure 1. Raman spectra for the as-deposited $SiO_{0.6}$ sample; the samples after annealing at 400, 700, and 1000 °C for 300 s and the pure SiO_2 control sample.

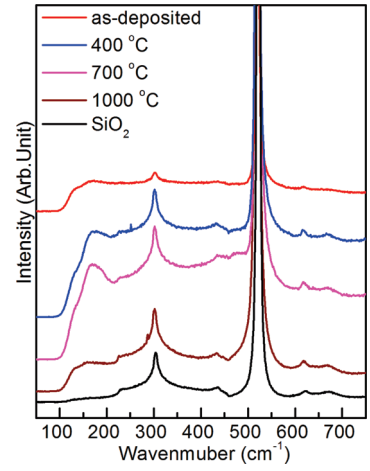

Figure 2. Raman spectra for the as-deposited $SiO_{1.4}$ sample; the samples after annealing at 400, 700, and 1000 °C for 300 s and the pure SiO_2 control sample.

3. Results and Discussion

3.1. Microstructure Characterization with Raman Spectra. ***3.1.1. Formation of Si Nanoclusters in the As-Deposited SiO_x Films as Revealed by Raman Spectra.*** Raman signals originate from the lattice vibrations in solids and relate directly to the microstructure of the materials. And it has been extensively employed to characterize both crystalline and amorphous Si.[24−26] Figure 1 and Figure 2 show the Raman spectra of the as-sputtered $SiO_{0.6}$ and $SiO_{1.4}$ samples and the samples after annealing at various temperatures, respectively. The Raman spectra of a pure SiO_2 films prepared by the same method is also presented for comparison purposes. Figure 3 shows a Raman spectrum from the SiO_x film deposited on normal glass substrate, which has no Raman signal in the

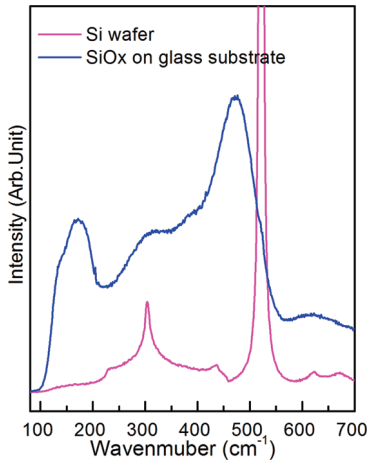

Figure 3. Raman spectra from the as-sputtered SiO_x sample deposited on normal glass substrate and the crystalline Si substrate.

concerned range and the Raman spectrum from the single crystalline Si substrate. The sharp peak located at ~520 cm^{-1} and the weak peak at ~300 cm^{-1} in Figures 1 and 2 originate from the phonon modes of crystalline Si.[24] These two crystalline Si Raman peaks were also clearly visible from the crystalline Si substrate, whereas they are absent in the Raman spectrum of the SiO_x films deposited on normal glass substrate as shown in Figure 3. Thus, these crystalline Si peaks in the as-deposited SiO_x samples were attributed to the crystalline silicon substrate. For pure SiO_2 films, the absence of other features except for the substrate peaks is because that the Raman efficiency of amorphous SiO_2 (a-SiO_2) is too low to give rise to detectable Raman signals, unless the a-SiO_2 film is sufficiently thick (thicker than several micrometers). In fact, for the as-deposited a-SiO_2 film with a thickness of about 300 nm, Raman signals scattering from the a-SiO_2 were hardly detected. However, for samples containing excess Si atoms, besides the substrate peaks, other features (broad Raman peaks) are observed, and the spectral features change depending on Si concentration. As can be observed from Figure 1, for the as-deposited $SiO_{0.6}$ sample, there is a transverse-optical (TO) band located at ~470 cm^{-1} and a transverse-acoustic (TA) band centered at ~160 cm^{-1}. These two broad Raman bands are the characteristic peaks of amorphous Si, scattering from the excess amorphous Si in the as-deposited films. This is in agreement with the results of several other researchers from different research groups who also have observed these two broad amorphous Si features in their Raman research of SiO_x films and attributed them to the formation of amorphous Si clusters.[25,26] For example, Nesheva et al.[25] reported that these two amorphous Si Raman features are absent for their as-deposited SiO_x samples by chemical vapor deposition when the annealing temperature is lower than 250°C due to the absence of amorphous Si domains and were clearly visible when the annealing temperature is higher (700 °C) due to the formation of small Si domain as a result of phase separation. Besides, Kanzawa et al.[27] demonstrated that small Si domains with a minimum size are required for detecting these amorphous Si Raman peaks in SiO_x films. That is why there is no distinguishable amorphous Si Raman peak in the Raman spectra of our as-sputtered $SiO_{1.4}$ sample as shown in Figure 2. It is possible that the amorphous Si nanoclusters in the as-sputtered $SiO_{1.4}$ are too small to give out detectable Raman signals due to the low Si concentration. However, as-compared with the pure SiO_2 sample, for the as-deposited $SiO_{1.4}$ sample, Si Raman intensity from 100−500 cm^{-1}, although not high, still can be observed, indicating the existence of amorphous Si phase. Moreover, in the Raman spectrum of the as-deposited SiO_x films, quite different from SiO_2 films, a high-frequency shoulder at around 550 cm^{-1} appears, extending up to 700 cm^{-1}. This high-frequency shoulder is also attributed to the Si nanocusters as suggested by Kanzawa et al.[27] Therefore, on the basis of the above interpretation, it is reasonable to assume that our as-sputtered SiO_x samples are chemically inhomogeneous, and there are amorphous Si nanoclusters formed during sputtering. The size of the amorphous Si nanoclusters depends on the Si concentration. In addition, the strong decrease of the 520 cm^{-1} band intensity (comparing with pure SiO_2 film) supports this suggestion as the absorption of amorphous Si in the blue wavelength region is significantly higher than that of Si oxides.

3.1.2. Effects of Annealing on the Si Nanoclusters. Si nanocrystals are usually induced by high temperature annealing of the amorphous SiO_x films. During annealing, significant structural changes take place due to the lattice relaxation, defect annihilation, and thermal decomposition of the Si suboxides. The Raman spectra of $Si_{0.6}$ and $SiO_{1.4}$ samples after annealing at various temperatures are also shown in Figures 1 and 2, respectively. It is apparent that the annealing leads to two types of variations in the Raman spectra. The first variation occurs when the annealing temperature is lower than 700 °C. There is a strong increase in the intensity of the amorphous Si Raman features. As discussed later (XPS results), the increase in the intensity of the amorphous Si Raman features is due to the increase in the amount of amorphous Si phase during annealing as a result of the thermal decomposition of Si suboxides. The XPS results (shown later) that show a strong increase in Si concentration after thermal processing will provide more solid evidence for the growth of Si nanoclusters. For high Si concentrations, particularly the $SiO_{0.6}$ sample, both the TO band located at ~470 cm^{-1}, and the TA band centered at ~160 cm^{-1} increase continuously with annealing temperature. For the low Si concentration $SiO_{1.4}$ sample, the TA band becomes distinguishable when the annealing is higher than 400 °C, but there is still lack of separated TO band. It is possible that the amorphous Si nanoclusters may be still not big enough to arise to a distinguishable TO band at this stage. However, as can be observed from Figure 2, for the $SiO_{1.4}$ sample annealed at 700 °C, the 520 cm^{-1} peak becomes asymmetric, with a low-frequency tail extending down to 450 cm^{-1}. Nesheva et al.[25] suggested this low-frequency tail resulted from the strong Raman scattering of the amorphous Si TO band at ~480 cm^{-1}. The second variation occurs when the annealing temperature is higher than 700 °C. Both the intensity of the TO band and the TA band decrease significantly. It has been concluded that the TO band at ~470 cm^{-1} originates from the destruction of the short-range order of the silicon lattice, i.e., from the bonding between nearest-neighbor atoms of the silicon lattice[24], while the TA band at ~160 cm^{-1} originates from the destruction of long- /or intermediate-range order of the Si lattice.[24] Thus the decrease in the intensity of the TO and TA bands indicates an annealing-induced lattice relaxation process, which reduces the average bond angle distortion and improves the long-range order of the Si lattice. When the annealing temperature is higher than 1000 °C, both TO and TA bands disappear because the amorphous Si nanoclusters transform into nanocrystalline Si with well-defined lattice.

3.2. Chemical Structure Characterization with XPS Spectrum. ***3.2.1. Chemical Structure of the As-Deposited SiO_x Film.*** Figures 4 and 5 shows the Si 2p XPS spectrum for the as-sputtered $SiO_{0.6}$ and $SiO_{1.4}$ samples and the samples after annealing at various temperatures, respectively. The Si 2p core-

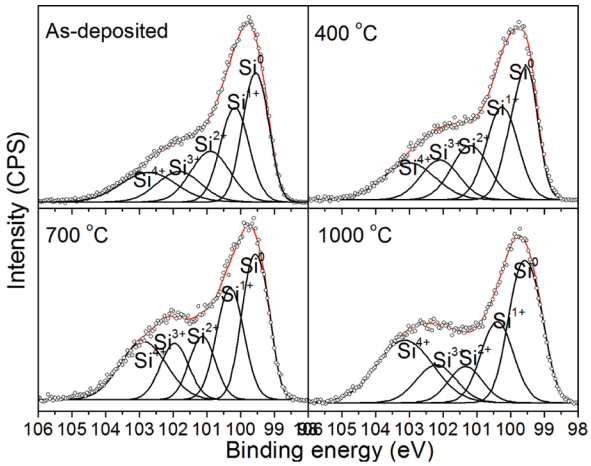

Figure 4. Si 2p XPS spectra for the as-deposited $SiO_{0.6}$ sample and the samples after annealing at 400, 700, and 1000 °C for 300 s.

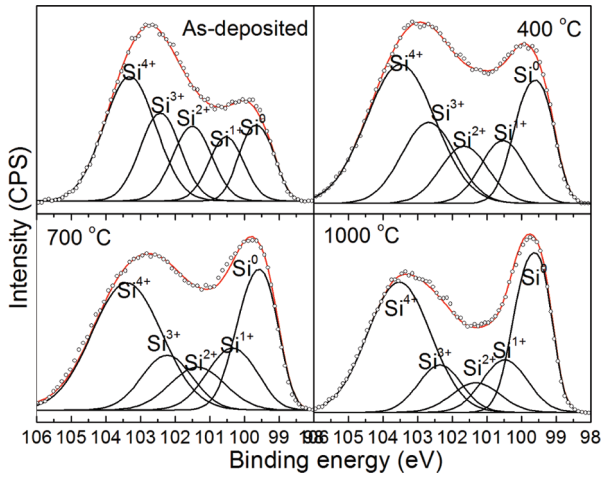

Figure 5. Si 2p XPS spectra for the as-deposited $SiO_{1.4}$ sample and the samples after annealing at 400, 700, and 1000 °C for 300 s.

level spectrum possesses two main peaks, corresponding to the $Si-Si_4$ and $Si-SiO_4$ tetrahedrons. Moreover, the Si 2p lines of both the Si^0 and Si^{4+} are not symmetrical and are separated by a flat region where the intensity does not drop to zero. Therefore, contributions from Si suboxides (Si^{1+}, Si^{2+}, and Si^{3+}) should be considered in order to account for the intensity level of the intermediate region. One should note that the SiO_x films were synthesized by reaction of the sputtered Si atoms with oxygen. It is quite possible that oxidation proceed with zero, one, two, three, or all four Si−Si bonds being replaced by Si−O bonds. We thus expect five components Si^0, Si^{1+}, Si^{2+}, Si^{3+}, and Si^{4+} in the films. This assumption is comparable to the RBM and also is the common chemical features at the Si/SiO_2 interface.[28] On the basis of this assumption, deconvolution of the XPS curves gives rise to 5 peaks, corresponding to Si^0, Si^{1+}, Si^{2+}, Si^{3+}, and Si^{4+}. The deconvolution was conducted with an popular procedures in this field and is similar to the approach of Rochet et al.[15] and Hohl et al.[23] These five chemical states were expected to be equally spaced from the binding energy of Si^0 to that of Si^{4+}. However, to take into account small differences in charging effects on the samples the peak energies were allowed to vary within 0.1 eV during the fitting process. The deconvolution of XPS curve was conducted by decomposing the Si 2p line into Si $2p^{1/2}$ and Si $2p^{3/2}$ lines with intensity ratio 1:2 and a fixed spin−orbit splitting of 0.6 eV as an atomic property. Only the sum of the Si $2p^{1/2}$ and $2p^{3/2}$ partner lines is shown for a clear presentation. The full width at half-maximum (2Γ) was assumed to be the same for both lines but allowed the variation from Si^0 to Si^{4+}, and the relative weight (W) was allowed to vary without constraint. The Si 2p XPS spectrum was fitted by a superposition of five Gaussian peaks (Si^0, Si^{1+}, Si^{2+}, Si^{3+}, and Si^{4+}), corresponding to no Si−Si bond, one Si−Si bond, two Si−Si bonds, three Si−Si bonds, or all four Si−Si bonds had been replaced by Si−O bonds.[23] The best fitting results was summarized in Table 1. As shown, there are sufficient Si suboxides in the as-deposited samples besides the Si and SiO_2 species, which shows a chemical feature predicted by RBM. The chemical structures yielded by XPS are further compared with the prediction by RBM (homogeneous Si rich oxide). The respective weights of the five chemical states calculated according to RBM are also show in Table 1. It shows that the calculated results from RBM can not be explained by the reconstruction of the samples spectrum we have made. Thus, despite the fact that the amorphous samples contain five Si chemical structures, there is still no complete agreement with the idealized random bonding statistics. On the other hand, a further comparison reveals that the weight of the Si^0 and Si^{4+} states are too high as compared to results from RBM, which is an appreciate mixture characteristic of a composite material consisting of two distinct Si and SiO_2 phases. Here, the XPS quantitative analysis, an alternative technique besides Raman microscopy, yields a direct proof for the previous argument that the as-deposited film is inhomogeneous, and there exists small Si phase regions. The XPS results also show an increase in Si^0 concentration with increasing Si concentration, indicating an increase in the size of the Si phase region. The results confirm our assumption based on Raman that the Si nanoclusters size is strongly affected by Si concentration. XPS depth profiling was conducted as shown in Figure 6. There are no obvious changes in the Si 2p and O 1s spectra at various depths, indicating the as-sputtered amorphous SiO_x film are uniform in composition.

3.2.2. Changes of Chemical Structure with Thermal Annealing. The XPS technique was again employed to examine the effects of annealing on the chemical structures. Si 2p XPS spectra of the $SiO_{0.6}$ and $SiO_{1.4}$ samples after annealing at various temperatures are also shown in Figures 4 and 5, respectively. It is clearly shown that the major effect of annealing on the chemical structures is to reduce the concentration of Si suboxides as well as to increase the content of Si and SiO_2. As shown in Table 1, there is a continuous increase in Si^0 and Si^{4+} concentration while a decrease in the Si suboxides concentration with annealing temperature. Quite similar evolution of chemical structure had also been found in reference 15. The changes in chemical structure are due to the fact that the Si suboxides were metastable and have a potential to thermally decompose into more stable Si and stoichiometric SiO_2 to reduce the enthalpy of the system during annealing by the following reaction[29]

$$SiO_x \rightarrow \left(1 - \frac{x}{2}\right)Si + \frac{x}{2}SiO_2 \qquad (1)$$

However, because the decomposition reaction need to overcome the energy barrier, thus to complete the reaction, long time and high temperature are needed. Therefore, there remain sufficient Si suboxides even after annealing at 1000 °C for 300 s. These Si suboxides may form a transition layer between the Si nanocluster and the oxide matrix, which have been confirmed by several other researchers.[15,18,23] The resulted Si^0 during annealing allows the rapid growth of the Si nanoclusters, which is consistent with the Raman spectral features. The diffusivity

TABLE 1: Comparison the Relative Weights of the Different Si Chemical States Yield by the XPS with that Calculated According to RBM

	$SiO_{0.6}$ (at %)					$SiO_{1.4}$ (at %)				
Si species	virgin	400 °C	700 °C	1000 °C	RBM	virgin	400 °C	700 °C	1000 °C	RBM
Si^0	30.37	32.57	35.53	37.16	23.38	16.43	20.02	25.74	28.71	0.98
Si suboxides	54.74	50.8	42.46	37.78	74.44	50.05	44.50	36.42	29.64	74.44
Si^{4+}	14.86	16.63	22.01	25.06	0.98	33.49	35.38	37.84	41.65	23.38

of Si in SiO_2 below 700 °C is less than the order of 10^{-19} cm^2/s,[30] thus for a 300 s treatment the diffusion lengths are only in the order of angstroms. This is not sufficient for the Si nanoclusters to grow. Thus diffusion should be not the dominant growth mechanism. However, thermal segregation of Si suboxides could provide rapid growth of Si nanoclusters, thus is considered the responsible mechanism. The segregation proceeds as percolation via "weak points" in the form of "Si creaks" or "Si breakdowns" in SiO_2. This does not need long-range diffusion and are very rapid.[30] Even so, as the annealing temperature of 700 °C is not sufficient to overcome the energy barrier for crystallization of Si clusters, the Si nanoclusters remain amorphous. During annealing at 1000 °C, the diffusivity of Si in SiO_2 increases to the order of 10^{-16} cm^2/s,[10] even this, for the 300 s treatment (with a diffusion length of 0.5−0.6 nm) is still not sufficient for all the excess Si atoms to diffuse into the crystalline boundaries. However, such high annealing temperature can provide sufficiently energy to self-organize the amorphous Si nanoparticles into more compact nc-Si with well-defined atomic lattices. On the other hand, it is quite possible that additional nucleation occurs through heterogeneous nucleation at the pre-existing defect sites where the threshold for nucleation is reduced by the energy released through the annihilation of the defect during annealing. However, once nucleation occurs with the formation of critically sized nuclei, the Si cluster growth is governed by the same phase segregation process as discussed above.

3.2.3. Formation of Si Nanoclusters in the As-Deposited SiO_x Films as Revealed by Valence Band XPS Spectra. Figures 7 and 8 show the valence band XPS spectra for the as-sputtered $SiO_{0.6}$ and $SiO_{1.4}$ samples and the samples after annealing at various temperatures, respectively. The valence band XPS spectra of a pure SiO_2 films prepared by the same method is also presented for comparison purpose. In the valence band of a-SiO_2 sample three groups of components can be distinguished. A feature labeled as A located at around the 6−7-eV energy range, corresponding to the O 2p lone-pair band. Two other components labeled with B and C, at higher binding energies, correspond to the strongly interaction of O 2p states with Si 3p and Si 3s level, respectively. In the case of the films with excess Si, besides these three groups, an additional group located at D 1−4 eV above its valence-band edge is found. The valence band XPS spectral features of SiO_x films show good agreement with theoretical calculation of silicon's valence band density of states.[31] The additional group D is attributed to the direct interaction of Si−Si bonding states (i.e., Si 3p) in SiO_x.[32] Previous results in the literature for SiO_x thin films with a chemical structure following the RBM show that the signal of group D can not be observed when the Si concentration is low (x values is higher than 1.0). Moreover, theoretical calculation also claimed that a minimum length of ∼10 atoms in the Si−Si

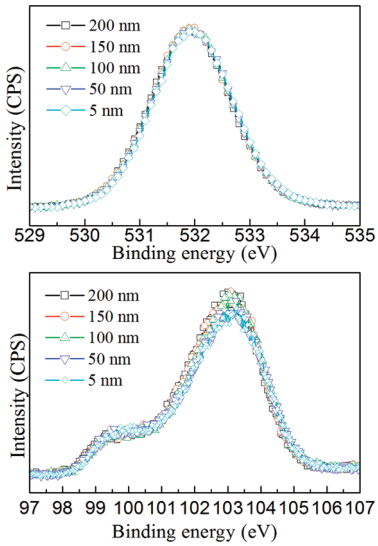

Figure 6. XPS depth profiling of the as-sputtered amorphous SiO_x film: (a) O 1s core level; (b) Si 2p core level.

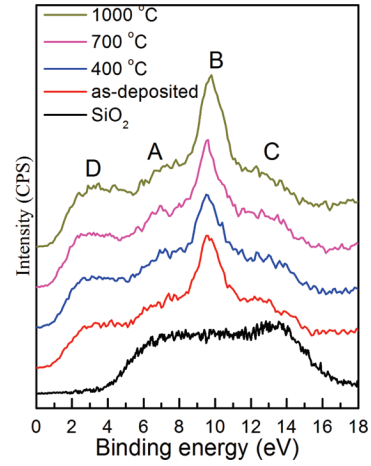

Figure 7. Valence-band XPS spectra for the as-deposited $SiO_{0.6}$ sample; the samples after annealing at 400, 700, and 1000 °C for 300 s and the pure SiO_2 control sample.

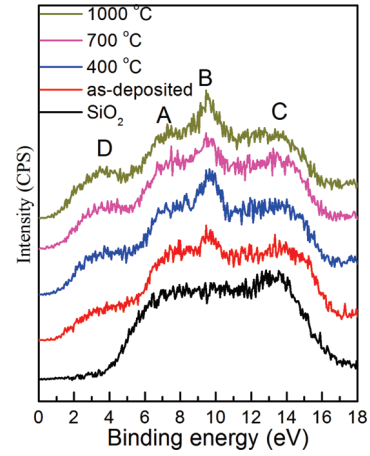

Figure 8. Valence-band XPS spectra for the as-deposited $SiO_{1.4}$ sample; the samples after annealing at 400, 700, and 1000 °C for 300 s and the pure SiO_2 control sample.

chains is required to observe this Si 3p states in the valence band.[33] However, the strong Si peaks intensity (group D) in the valence band XPS spectra even is noticeable in the spectra for our samples with very low Si concentration sample ($SiO_{1.4}$). Therefore, the valence band spectral features strongly suggest the formation of Si−Si long chains (Si clusters) in the films. Furthermore, as can be seen that the intensity of group D of the as-deposited $SiO_{0.6}$ is higher than that of the as-deposited $SiO_{1.4}$. The high intensity and broaden of group D imply that the probability that a given Si is surrounded by other Si atoms has increased, so does the probability of interaction between silicon orbitals,[15] indicating an increase in the size of the Si nanoclusters with increasing Si concentration. The intensity of group D also increases with annealing temperature for both samples. This increase intensity is due to growth of the Si nanoclusters during annealing.

3.3. Formation Mechanism of Si Nanoclusters in the As-Deposited SiO_x Films. The formation of the amorphous Si clusters in the SiO_x films is speculated to be related to the high kinetic energy of the sputtered Si atoms. During sputtering, parts of the sputtered Si atoms react with oxygen atoms with either full oxidization to form SiO_2 or partially oxidization to form Si suboxides; on the other hand, certain sputtered Si atoms are not oxidized because of the deficient oxygen ambient during sputtering. These nonoxidized Si can deposit on the substrate directly. The mean free path of the sputtered particles can be estimated with eq 2[34]

$$\lambda_a \approx \frac{1}{\pi(r_A + r_B)^2 n_B} \quad (2)$$

where r_A corresponds to the atomic radius of a sputtered particle and r_B corresponds to the atomic radius of Ar; n_B is the particle density ($N/V = P/kT$) of Ar in the chamber. r_{Ar} is 0.191 nm; r_{Si} is 0.110 nm. Note that the chamber pressure was 0.2 Pa, and the chamber temperature was 323 K. For the nonoxidized Si atoms, the mean free paths were calculated to be 7 cm. At a target-to-substrate distance of 8 cm, this corresponds to a probability that 50% sputtered silicon atoms reach the substrate without any collisions. Thus, a significantly higher fraction of energetic sputtered silicon particles (1−2 eV) arrive at the substrate without kinetic energy loss. On the one hand, the high kinetic energy enables the sputtered silicon atoms to migrate on the growing films surface to form nanosized Si clusters; on the other hand, the bombardment of the energetic particles on the growing films surface accelerate this surface migration, also promoting the formation of the Si nanoclusters.

3.4. Microstructure of the As-Deposited SiO_x Films. For the nanoscale microstructures, the as-deposited SiO_x films show features of both RBM (five chemical structures) and RMM (ultrahigh concentration of Si and SiO_2 species). Similar chemical structures have been reported by Hohl et al.[23] For their bulk amorphous SiO_x, an interface clusters mixtures model to describe the microstructure of bulk amorphous silicon monoxide has been proposed. It is depicted that the amorphous bulk SiO has a complex structure consisting of nanoscale regions of Si and SiO_2, which are separated by a layer of Si suboxides. However, this may not be the case for amorphous SiO_x thin films. For the Si atoms reacting with oxygen, the Si atoms will bond to one or more (up to four) oxygen atoms once sputtered out of the Si target. On one hand, the introduction of Si−O bond will increase the size of the particles, i.e., the more Si−O bonds, the larger of the particle radius. Moreover, the mean free paths significantly decrease, which means that the probabilities of the sputtered particles reach the substrate without any collision decrease. Here, we define the sputtered Si atoms into three categories: (1) silicon in the forms of silica, (2) silicon in the suboxide states, and (3) silicon in the forms of pure Si. For SiO_2 particles, they will reach the substrate without surface migration to form the matrix of the SiO_x films. As for the Si suboxides, since sufficient (almost half of the content) Si atoms are in the forms of Si suboxies, one should not take them to be the interface layer (usually with a thickness of several atomic layers) between Si clusters and SiO_2 matrix. However, they may form a transition layer between the Si clusters and the SiO_2 matrix to reduce the lattice distortion. This transition layer may form a shell of the Si clusters with increasing oxidation states far along from the Si clusters core.

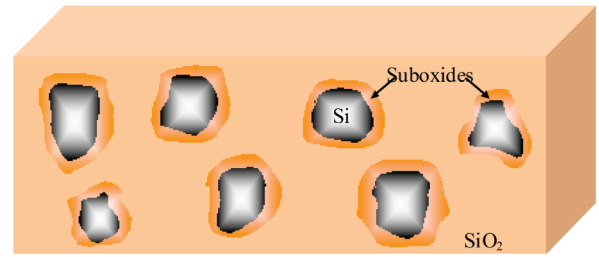

Figure 9. Schematic diagram of the microstructure of the as-deposited amorphous SiO_x films.

On the basis of the above discussion, we speculate that the microstructure of the as-deposited films as follows. The microstructure of amorphous SiO*x* films contains Si cluster core with suboxides shell domains, which themselves embedded in the SiO_2 matrix as shown in Figure 9. The Si cluster core can have a different sizes; thus the Si cluster core with suboxides shell domains. The average size of the domains may depend on the total Si concentration of the films.

4. Conclusion

The microstructure of magnetron sputtered amorphous SiO_x films were studied by a combination of XPS and Raman microscopy. XPS results reveal that the bonding configurations of amorphous SiO_x films show the features of both Random bonding model and Random mixture model: five Si chemical states were found with ultrahigh concentration of Si^0 and Si^{4+}. Raman spectra and valence band XPS spectra suggest the formation of amorphous Si nanoclusters in the as-sputtered amorphous SiO_x films. The formation of amorphous Si nanoclusters was attributed to the high kinetic energy and surface migration of the sputtered Si atoms. The nanoscale structure of the as-sputtered SiO_x consists of nanoclusters of Si cores with suboxides shell which themselves embedded in the SiO_2 matrix.

References and Notes

(1) Chen, X. Y.; Lu, Y. F.; Wu, Y. H.; Cho, B. J.; Tang, L. J.; Lu, D.; Dong, J. R. *Appl. Surf. Sci.* **2006**, *253*, 2718.
(2) Iacona, F.; Bongiorno, C.; Spinella, C.; Boninelli, S.; Priolo, F. *J. Appl. Phys.* **2004**, *95*, 3723.
(3) Fang, Y. C.; Li, W. Q.; Qi, L. J.; Li, L. Y.; Zhao, Y. Y.; Zhang, Z. J.; Lu, M. *Nanotechnology* **2004**, *15*, 494.
(4) Lu, Y. W.; Du, X. W.; Hu, S. L.; Han, X.; Li, H. *Appl. Phys. Lett.* **2007**, *90*, 241910.
(5) Vivas Hernandez, T. V. T.; Quintos Vasquez, A. L.; Matsumoto, Y.; Khomenkova, L.; Shcherbina, L. *J. Phys.: Conf. Ser.* **2007**, *61*, 1231.
(6) Wang, J.; Wang, X. F.; Li, Q.; Hryciw, A.; Meldrum, A. *Philos. Mag.* **2007**, *87*, 11.
(7) Liu, Y.; Chen, T. P.; Ding, L.; Zhang, S.; Fu, Y. Q.; Fung, S. *J. Appl. Phys.* **2006**, 100.

(8) Franzo, G.; Irrera, A.; Moreira, E. C.; Miritello, M.; Iacona, F.; Sanfilippo, D.; Di Stefano, G.; Fallica, P. G.; Priolo, F. *Appl. Phys. A* **2002**, *74*, 1.

(9) Liu, Y.; Chen, T. P.; Fu, Y. Q.; Tse, M. S.; Hsieh, J. H.; Ho, P. F.; Liu, Y. C. *J. Phys. D* **2003**, *36*, L97.

(10) Nesbit, L. A. *Appl. Phys. Lett.* **1985**, *46*, 38.

(11) Daldosso, N.; Luppi, M.; Ossicini, S.; Degoli, E.; Magri, R.; Dalba, G.; Fornasini, P.; Grisenti, R.; Rocca, F.; Pavesi, L.; Boninelli, S.; Priolo, F.; Spinella, C.; Iacona, F. *Phys. Rev. B* **2003**, *68*, 8.

(12) Seifarth, H.; Grotzschel, R.; Markwitz, A.; Matz, W.; Nitzsche, P.; Rebohle, L. *Thin Solid Films* **1998**, *330*, 202.

(13) Thogersen, A.; Diplas, S.; Mayandi, J.; Finstad, T.; Olsen, A.; Watts, J. F.; Mitome, M.; Bando, Y. *J. Appl. Phys.* **2008**, 103.

(14) Ternon, C.; Dufour, C.; Gourbilleau, F.; Rizk, R. *Eur. Phys. J. B* **2004**, *41*, 325.

(15) Rochet, F.; Dufour, G.; Roulet, H.; Pelloie, B.; Perriere, J.; Fogarassy, E.; Slaoui, A.; Froment, M. *Phys. Rev. B* **1988**, *37*, 6468.

(16) Inokuma, T.; Wakayama, Y.; Muramoto, T.; Aoki, R.; Kurata, Y.; Hasegawa, S. *J. Appl. Phys.* **1998**, *83*, 2228.

(17) Serincan, U.; Kulakci, M.; Turan, R.; Foss, S.; Finstad, T. G. *Nucl. Instrum. Meth. Phys. Res. Sec. B* **2007**, *254*, 87.

(18) Kanemitsu, Y.; Ogawa, T.; Shiraishi, K.; Takeda, K. *Phys. Rev. B* **1993**, *48*, 4883.

(19) Park, N. M.; Kim, T. S.; Park, S. J. *Appl. Phys. Lett.* **2001**, *78*, 2575.

(20) Qin, G. G.; Li, A. P.; Zhang, B. R.; Li, B. C. *J. Appl. Phy.* **1995**, *78*, 2006.

(21) Philipp, H. R. *J. Non-Cryst. Solids* **1972**, *8*−*10*, 627.

(22) Temkin, R. J. *J. Non-Cryst. Solids* **1975**, *17*, 215.

(23) Hohl, A.; Wieder, T.; van Aken, P. A.; Weirich, T. E.; Denninger, G.; Vidal, M.; Oswald, S.; Deneke, C.; Mayer, J.; Fuess, H. *J. Non-Cryst. Solids* **2003**, *320*, 255.

(24) Zhang, P. X.; Mitchell, I. V.; Tong, B. Y.; Schultz, P. J.; Lockwood, D. J. *Phys. Rev. B* **1994**, *50*, 17080.

(25) Nesheva, D.; Raptis, C.; Perakis, A.; Bineva, I.; Aneva, Z.; Levi, Z.; Alexandrova, S.; Hofmeister, H. *J. Appl. Phys.* **2002**, *92*, 4678.

(26) Daldosso, N.; Das, G.; Larcheri, S.; Mariotto, G.; Dalba, G.; Pavesi, L.; Irrera, A.; Priolo, F.; Iacona, F.; Rocca, F. *J. Appl. Phys.* **2007**, *101*, 113510.

(27) Kanzawa, Y.; Hayashi, S.; Yamamoto, K. *J. Phys.-Condens. Matter* **1996**, *8*, 4823.

(28) Lucovsky, G. *J. Non-Cryst. Solids* **1998**, *227*−*230*, 1.

(29) Barranco, A.; Yubero, F.; Espinos, J. P.; Holgado, J. P.; Caballero, A.; Gonzalez-Elipe, A. R.; Mejias, J. A. *Vacuum* **2002**, *67*, 491.

(30) Kachu, G. A.; Zhuravlev, K. S.; Pazdnikov, N. A.; Leier, A. F.; Tyschenko, I. E.; Volodin, V. A.; Skorupa, W.; Yankov, R. A. *Nucl. Instrum. Meth. Phys. Res. Sec. B* **1997**, *127*−*128*, 583.

(31) Kroll, P.; Schulte, H. J. *Phys. Status Solidi B* **2006**, *243*, R47.

(32) Rochet, F.; Rigo, S.; Froment, M.; Danterroches, C.; Maillot, C.; Roulet, H.; Dufour, G. *Adv. Phys.* **1986**, *35*, 237.

(33) Barranco, A.; Yubero, F.; Espinos, J. P.; Groening, P.; Gonzalez-Elipe, A. R. *J. Appl. Phys.* **2005**, 97.

(34) Hidetoshi; Miyazaki., *Jap. J. Appl. Phys.* **2008**, *46*, 3766.

JP906284F